Nano Research

ISSN 1998-0124 CN 11-5974/O4
https://doi.org/10.1007/s12274-022-4314-6

Research Article

Intrinsically patterned corrals in monolayer Ag_5Se_2 and selective molecular co-adsorption

Jianchen Lu[1,4,§], Shiru Song[1,§], Shuai Zhang[1,§], Yang Song[1,§], Yun Cao[1], Zhenyu Wang[1], Li Huang[1], Hongliang Lu[1,3], Yu-Yang Zhang[1,3], Sokrates T. Pantelides[1,2], Shixuan Du[1,3] (✉), Xiao Lin[1,3] (✉), and Hong-Jun Gao[1,3] (✉)

[1] *Institute of Physics & University of Chinese Academy of Sciences, Chinese Academy of Sciences, Beijing 100190, China*
[2] *Department of Physics and Astronomy and Department of Electrical Engineering and Computer Science, Vanderbilt University, Nashville, TN 37235, USA*
[3] *CAS Center for Excellence in Topological Quantum Computation, Chinese Academy of Sciences, Beijing 100190, China*
[4] *Faculty of Materials Science and Engineering, Kunming University of Science and Technology, Kunming, Yunnan 650093, China*
[§] *Jianchen Lu, Shiru Song, Shuai Zhang, and Yang Song contributed equally to this work.*

Received: 31 August 2021 / **Revised:** 7 February 2022 / **Accepted:** 11 March 2022

ABSTRACT

Functionalized two-dimensional (2D) materials play an important role in both fundamental sciences and practical applications. The construction and precise control of patterns at the atomic-scale are necessary for selective and multiple functionalization. Here we report the fabrication of monolayer pentasilver diselenide (Ag_5Se_2), a new type of intrinsically patterned 2D material, by direct selenization of a Ag(111) surface. The atomic arrangement is determined by a combination of scanning tunneling microscopy (STM), low-energy electron diffraction (LEED), and density-functional-theory (DFT) calculations. Large-scale STM images exhibit a quasi-periodic pattern of stoichiometric triangular domains with a side length of ~ 15 nm and apical offsets. The boundaries between triangular domains are sub-stoichiometric. Deposition of different molecules on the patterned Ag_5Se_2 exhibits selective adsorption behavior. Pentacene molecules preferentially adsorb on the boundaries, while tetracyanoquinodimethane (TCNQ) molecules adsorb both on the boundaries and the triangular domains. By co-depositing pentacene and TCNQ molecules, we successfully construct molecular corrals with pentacene on the boundaries encircling TCNQ molecules on the triangular domains. The realization of epitaxial large-scale and high-quality, monolayer Ag_5Se_2 extends the family of intrinsically patterned 2D materials and provides a paradigm for dual functionalization of 2D materials.

KEYWORDS

two-dimensional materials, dual functionalization, scanning tunneling microscope, epitaxial growth, Ag_5Se_2 monolayer

1 Introduction

Since the discovery of graphene, two-dimensional (2D) materials attract intense attention due to their novel properties [1–5] and potential applications [6–8]. 2D materials often possess properties that are quite different from their bulk counterparts [9, 10]. For example, monolayer $MoSe_2$ features a direct bandgap compared with an indirect bandgap in the bulk form [11, 12]; unlike the bulk form, a 2D MoS_2 nanosheet can serve as an efficient catalyst for hydrogen-evolution reactions [13]. Functionalization of 2D materials, which further enhances their versatility and applications, can be realized in several ways, such as intercalation [14], doping [15], molecular adsorption [16], and covalent functionalization [17].

To achieve selective functionalization by adsorbates, moiré patterns, which originate from lattice mismatch between the substrate and the 2D material, have been widely used [18]. For instance, at low coverage, pentacene molecules mainly adsorb on the face-centered cubic (fcc) regions of the moiré patterns formed on a graphene/Ru(0001) structure [19]. Copper phthalocyanine (CuPc) molecules and Xe atoms get trapped by dipole rings on a boron nitride nanomesh formed on Rh(111) [20]. Recently, there have been reports of intrinsically patterned 2D materials, e.g., $PtSe_2$ monolayers featuring alternating 1H and 1T triangles, CuSe monolayers featuring periodic arrays of triangular nanopores [21], and VSe_2 monolayers featuring one-dimensional (1D) sub-stoichiometric chains [22]. Some of them show that individual atoms or molecules can be selectively adsorbed at particular regions [21–23]. Though selective adsorption behavior has been reported when two species were deposited on metal substrate [24], the selective adsorption on 2D materials remains a challenge when co-adsorption of two or more species.

In this paper, we report the fabrication of an intrinsically patterned 2D material, Ag_5Se_2, exhibiting the possibility of dual functionalization. Ag_5Se_2 was prepared by direct selenization of Ag(111) [10, 25, 26], i.e., depositing selenium on the silver substrate and annealing in ultrahigh-vacuum (UHV). The as-formed monolayer Ag_5Se_2 features triangular patterns, ~ 15 nm in size, with apical offsets. The atomic structure of the triangular domains features a hexagonal lattice, confirmed by low-energy-electron diffraction (LEED), scanning tunneling microscopy (STM), and density/functional-theory (DFT) calculations. The

Address correspondence to Shixuan Du, sxdu@iphy.ac.cn; Xiao Lin, xlin@ucas.ac.cn; Hong-Jun Gao, hjgao@iphy.ac.cn

structure of the triangular-domain boundaries was determined by combining atomically resolved STM images and DFT calculations. The hexagon orientations in adjacent domains are the same, but a relative shift between domains that is induced by the substrate leads to the distinct domain boundaries. Finally, the adsorption behaviors of several kinds of molecules on Ag_5Se_2 have been investigated. Pentacene molecules preferentially adsorb on the boundaries, while tetracyanoquinodimethane (TCNQ) molecules do not exhibit selectivity, adsorbing both on the boundaries and terraces and disturbing the boundary network. Nevertheless, we find that co-deposition of pentacene and TCNQ leads to pentacene-decorated boundaries and TCNQ on the terraces, forming molecular corrals. This kind of co-deposition of two molecules is a new paradigm that may lead to successful dual functionalization of intrinsically patterned 2D materials.

2 Results and discussion

The fabrication process of the sample is illustrated in Fig. 1(a). Selenium atoms are deposited on the Ag(111) substrate and the sample is annealed (see the Experimental Section for more details). A typical large-area STM image shown in Fig. 1(b) indicates that the material is intrinsically patterned. The surface is divided into many triangular domains ~ 15 nm in size (one of the triangles is highlighted by a black triangle in Fig. 1(b)) with apical offsets (indicated by a black dotted circle).

Figure 2(a) presents a magnified STM image of triangular patterns. The orientations of the silver substrate (Ag[1$\bar{1}$0] and Ag[11$\bar{2}$]) are labelled by black arrows. The bright dots in the image, some of which are marked by purple arrows, are likely to be clusters of unreacted Se atoms. An atomically resolved zoom-in STM image in one triangular domain, indicated by a dashed rectangle in Fig. 2(a), is displayed in Fig. 2(b), clearly revealing a well-ordered honeycomb-like structure (marked by a colored hexagon). One unit cell of the honeycomb lattice is represented by a blue rhombus in Fig. 2(b). Based on STM measurements, the angles between the lattice orientations of the unit cell (the blue rhombus) and the silver substrate direction [1$\bar{1}$0] (black arrow) are 19° and 41°, while the side of the blue rhombus is ~ 7.6 ± 0.2 Å. These STM measurements, as well as the LEED results shown in Fig. S1 in the Electronic Supplementary Material (ESM), reveal that the honeycomb lattice forms a $(\sqrt{7}\times\sqrt{7})R19.1$ superstructure with respect to the Ag(111) substrate.

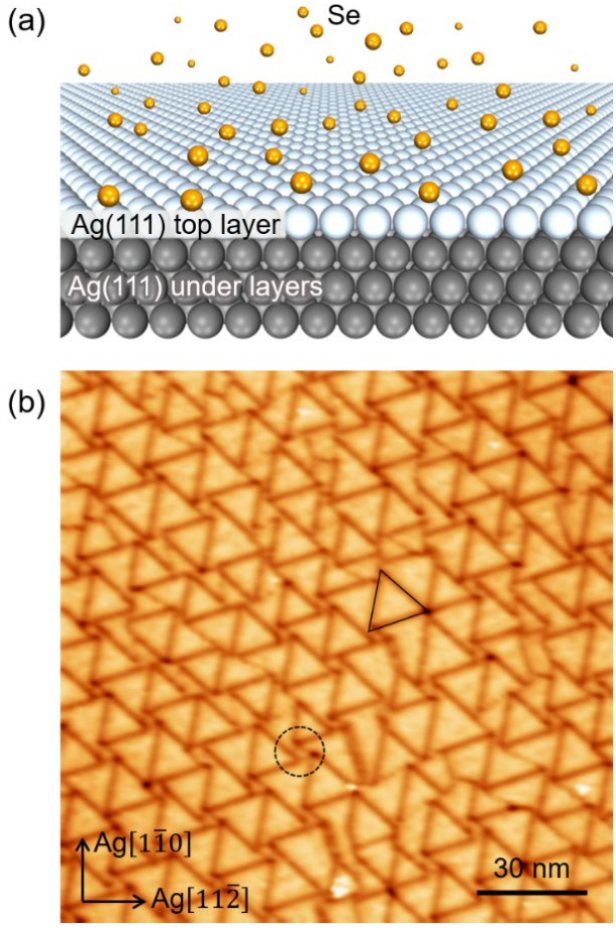

Figure 1 Large-area STM image of Se atoms deposited on a Ag(111) substrate. (a) Schematic illustration of the growth process. (b) Large-scale STM image shows triangular domains (V_s = –2.0 V and I_t = 0.2 nA). The black triangle is a guide to the eye. The black dotted circle marks the apical connection of several triangular domains.

In order to explore the atomic configurations, we built three models (Fig. 2(c) and Figs. S2(a) and S2(b) in the ESM) and did corresponding STM simulations in an effort to match the atomically resolved STM image shown in Fig. 2(b). By comparing the distance between the neighboring bright spots and the height of the bright features, we found that the DFT-optimized model and the corresponding STM simulation of a Ag_5Se_2 monolayer (Figs. 2(c) and 2(d)) agree well with the STM image of Fig. 2(b). Figure 2(c) shows the top and side view of a fully relaxed atomic geometry for Ag_5Se_2/Ag(111). The 2D unit cell of monolayer Ag_5Se_2 is outlined with a blue rhombus. There are seven atoms per unit cell, two selenium atoms, and five silver atoms. The Se atoms in the Ag_5Se_2 monolayer form a honeycomb-like structure, as indicated by the colorful hexagon, with different colored sides representing different lengths. More specifically, the silver atoms in the Ag_5Se_2 layer follow the structure and directions of the Ag substrate. In other words, the structure of the monolayer Ag_5Se_2 could be considered as a Ag(111) surface with periodic replacement of two adjacent Ag atoms with two Se atoms but having a small offset in the opposite directions. The offset can be clearly identified in the zoom-in atomic structure of Ag_5Se_2 as shown in Fig. S3(b) in the ESM, where the paired Se atoms do not exactly sit on the high-symmetry sites of the Ag(111) substrate, but have a small offset. Figure S3(c) in the ESM is the corresponding side view of Ag_5Se_2/Ag(111) system, which demonstrates the vertical distance of monolayer Ag_5Se_2 relative to the substrate. Based on this optimized structure of Ag_5Se_2/Ag(111), an STM image was simulated at the sample bias of –0.5 V as shown in Fig. 2(d). Only the left part of Fig. 2(d) is overlaid by the atomic model for clarity. The overall features in the simulated STM image (Fig. 2(d)) are in excellent agreement with the experimental STM image (Fig. 2(b)), confirming the model of the (1×1) $Ag_5Se_2/(\sqrt{7}\times\sqrt{7})$ Ag(111).

Figure 3(a) is a typical STM image showing several triangular domains with sides measuring ~ 15 nm. Figure 3(b) is a zoom-in STM image from Fig. 3(a), showing the highly resolved domain-boundary structure. An armchair-edge configuration is clearly identified, as indicated by the blue and black hexagons in Fig. 3(b). The two domains (domain 1 and domain 2) in Fig. 3(b) have the same structure and the same orientations, but with a shift, resulting in a domain boundary.

To figure out the atomic configuration of the highly ordered boundary, we carried out DFT calculations. We built a slab model in a large supercell of (13.20×45.70) with an intersection angle of 95.2°, as shown in Fig. S4 in the ESM. Figure 3(c) is the top view of the relaxed model of a boundary. To make the boundary configuration more explicit, the atomic structure of the two domains is superimposed by hexagons formed by Se atoms. There are two noteworthy characteristics in the Ag_5Se_2 boundary

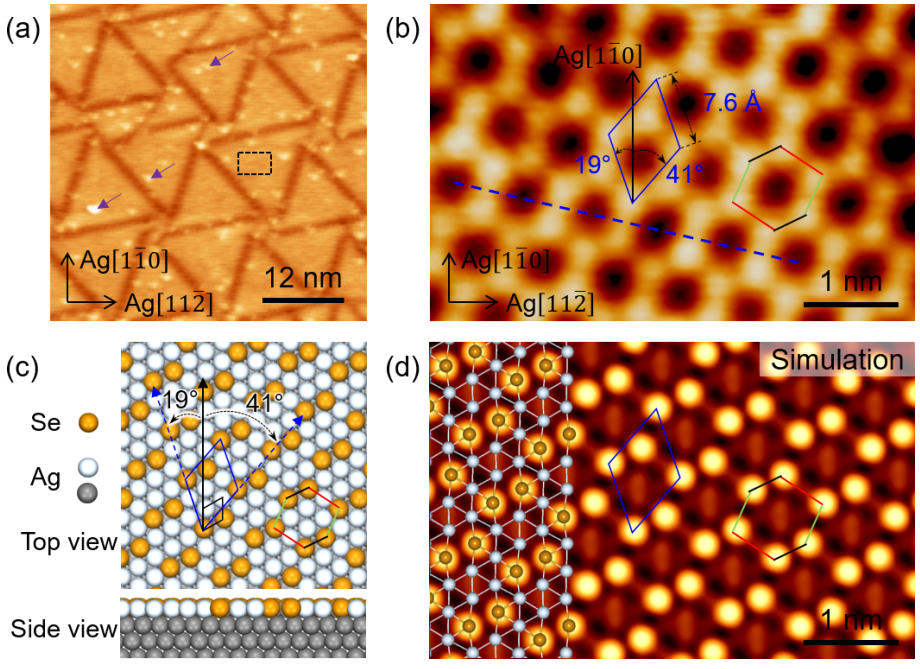

Figure 2 STM images, atomic structure, and STM simulation of the honeycomb lattice on Ag(111). (a) A zoom-in large-scale STM image of the triangular pattern on Ag(111) (V_s = – 3 V and I_t = 0.5 nA). (b) Zoom-in, atomically resolved STM image of the dotted rectangle in (a) (V_s = – 0.05 V and I_t = 1.0 nA). The multicolor hexagon illustrates the honeycomb-like structure and the blue rhombus represents the 2D primitive unit cell of the honeycomb lattice with a side of 7.6 ± 0.2 Å. (c) DFT optimized atomic model of the honeycomb lattice containing five silver and two selenium atoms in one unit cell (Ag_5Se_2) on the Ag(111) substrate. (d) Corresponding simulation image with the atomic model overlaid at the left part.

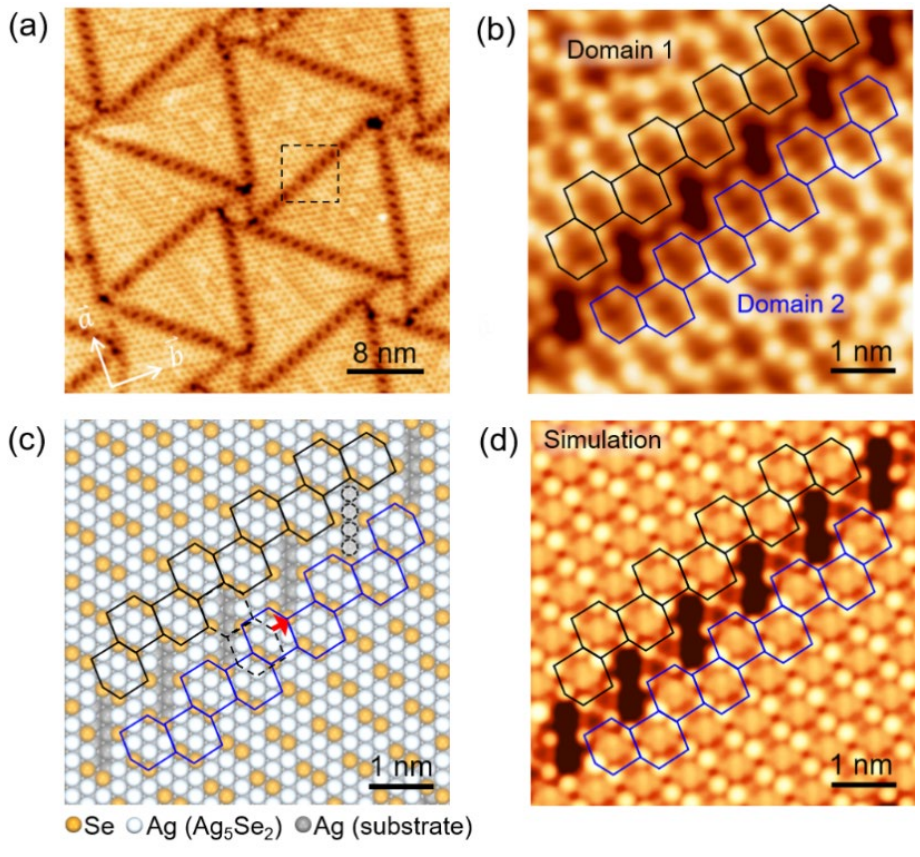

Figure 3 Domain-boundary structure of monolayer Ag_5Se_2. (a) STM image of Ag_5Se_2/Ag(111) shows triangular domains with ordered boundaries. (V_s = –2.0 V and I_t = 0.2 nA) (b) Atomically resolved STM image clearly reveals the structure of the domain boundary. Black and blue hexagons indicate the hexagons from Domain 1 and Domain 2, respectively. (V_s = –0.5 V and I_t = 1.5 nA) (c) DFT-calculated atomic model of Ag_5Se_2 boundary. The dashed hexagons and the red arrow indicate the shift between domain 1 and domain 2. Four black dotted circles indicate the four missing silver atoms in a domain boundary. Detail information about the formation of boundary can be found in Fig. S5 in the ESM. (d) Simulated STM image of the boundary based on (c) agrees well with the experimental image in (b).

configuration. First, the shift from domain 1 to domain 2 is a distance between two nearest silver atoms as indicated by black dashed hexagons and the red arrow in Fig. 3(c). The shifting distance is the bond length of Ag–Ag. Figure S5 in the ESM shows detail information of boundary formation. Second, there are seven extra silver atoms between two domains and four of them missing

in the dark regions as marked by black dotted circles in Fig. 3(c), which correspond to the black holes on the boundary in the STM image (Fig. 3(b)). On the basis of the domain-boundary structure in Fig. 3(c), we obtained a simulated STM image (Fig. 3(d)) that agrees well with the experimental STM image (Fig. 3(b)). In addition, our q-Plus atomic force microscopy (AFM) measurements of monolayer Ag_5Se_2 on Ag(111) substrate (Fig. S6 in the ESM) confirm that the boundary is indeed missing some atoms. Furthermore, the stoichiometric ratio of the domain is 5:2 (Ag:Se), while that of the domain boundary is 7:4 (Ag:Se) (Fig. S5 in the ESM). The loss of Ag atoms at domain boundaries indicates that the replacement of Se atoms with Ag atoms introduces strain in the monolayer Ag_5Se_2. In other words, Ag atoms are periodically squeezed out to release the strain, and the Ag vacancies synchronously form at domain boundaries. It is a common phenomenon in the growth process of material to release strain by losing some atoms. For example, the growth of monolayer CuSe on Cu(111) exhibits the distinct parallelogram-shaped nanopores formed by losing 13 atoms [21].

In order to investigate electronic property of the monolayer Ag_5Se_2 on Ag(111) substrate, we performed the scanning tunneling spectroscopy (STS) measurement at the domain boundary and terrace of the monolayer Ag_5Se_2. Both the dI/dV curves acquired at the boundary and terrace show a "U" shape at the bias voltage of –2 to 2 V shown in Fig. S7(b) in the ESM. The main difference between two dI/dV curves is reflected in the positive bias voltage, where the intensity of the dI/dV curve obtained at the boundary is stronger than that at the terrace. At a smaller voltage range of –1 to 1 V and –0.5 to 0.5 V, two dI/dV curves show same behaviour shown in Figs. S7(c) and S7(d) in the ESM. In addition, it should be noted that there are still some electronic state at the Fermi level, indicating a metallic feature for monolayer Ag_5Se_2 on Ag(111) substrate. In order to further investigate the electronic properties of the monolayer Ag_5Se_2 on Ag(111) substrate, we performed the DFT calculation. Figure S8 in the ESM shows the calculated density of states for monolayer Ag_5Se_2 on Ag(111) substrate. The calculation results indicate metallic behaviours for both the terrace and boundary, and projected density of states on the terrace and boundary are no obvious difference.

The quasi-periodic triangular pattern of Ag_5Se_2/Ag(111) is an ideal natural template for selective adsorption of molecules. Two kinds of molecules, a non-polar, chain-like pentacene molecule, and a relatively small and polar TCNQ molecule, have been chosen and deposited on the monolayer Ag_5Se_2 samples. Figure 4(a) shows the adsorption behavior of the pentacene molecules. All pentacene molecules adsorb on the boundaries of the triangular domains. The size of pentacene fits the holes in the boundary very well, which makes pentacene lie exactly on the hole and in good alignment. DFT calculations show the binding energy per pentacene molecule on a boundary (2.34 eV) is larger than that on the triangular domains (2.23 eV). Thus, pentacene molecules prefer the boundaries, in accord with experimental observations. As illustrated in Fig. 4(b), TCNQ molecules do not show specific selectivity on different sites of Ag_5Se_2, and adsorb both on the terraces and boundaries. DFT calculations show that the binding energy per TCNQ molecule on a boundary (2.63 eV) is only slightly larger than that on triangular domains (2.58 eV), which is also in agreement with experimental results if the thermal effect is taken into account.

In addition to the above experiments in which a single molecular species is adsorbed on the patterned surface, we designed an experiment to co-deposit different molecules, and finally fabricated molecular corrals [27]. The schematic model is

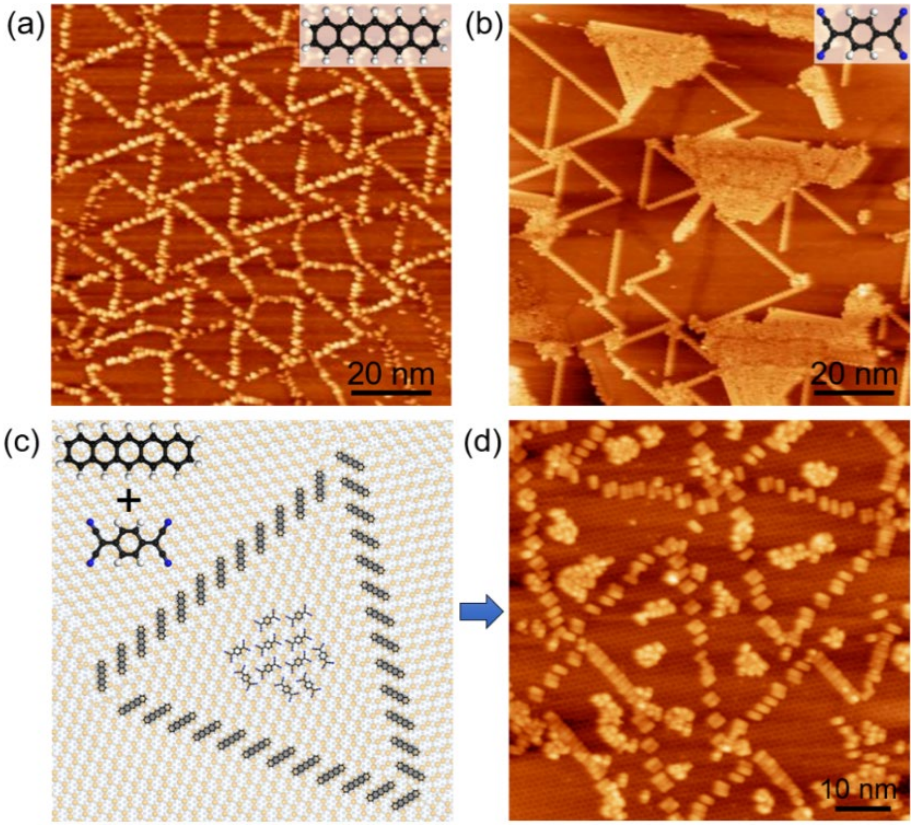

Figure 4 Adsorption behaviors of organic molecules on Ag_5Se_2/Ag(111). (a) Pentacene molecules preferentially adsorb on the boundaries (V_s = –1 V and I_t = 0.05 nA). (b) TCNQ molecules adsorb randomly, both on the boundaries and on the triangular domains (V_s = –2.5 V and I_t = 0.05 nA). (c) Schematic diagram of two molecules (Pentacene and TCNQ) adsorption on Ag_5Se_2. (d) Pentacene molecules adsorbed on the boundaries form molecular corrals surrounding the TCNQ molecules. (V_s = –1 V and I_t = 0.05 nA).

shown in Fig. 4(c). Pentacene molecules occupy the boundaries and TCNQ molecules are encircled on the triangular domain, forming a molecular corral. Experimentally, pentacene molecules are deposited first to occupy the boundaries, which restricts TCNQ molecules to subsequently adsorb solely on the triangular domains (Fig. 4(d)). However, if we invert the deposition sequence, TCNQ molecules adsorb both on the boundaries and the triangular domains, while pentacene molecules adsorb only on the uncovered boundaries.

3 Conclusions

Ag_5Se_2, a new 2D material, was synthesized by direct selenization on Ag(111). The Ag_5Se_2 monolayer exhibits a triangular pattern with a side length of ~ 15 nm and apical offsets. Besides, the pattern enables selective adsorption of different molecules. We demonstrated that co-adsorption of pentacene and TCNQ molecules leads to the formation of molecular corrals. This newly developed approach is yet another step toward the fabrication of molecular devices.

4 Methods

Sample preparations and *in-situ* characterizations. Experiments were performed in an ultrahigh vacuum (UHV) LT-STM system (Omicron) with a base pressure better than 2×10^{-10} mbar. This system was equipped with a preparation chamber, LEED, and STM. Single-crystal Ag(111) (MaTecK) substrate was cleaned by several cycles of Ar^+ sputtering and annealing, until it yielded a distinct Ag(1 × 1) diffraction spots in the LEED pattern and clean terraces in STM images. Pure selenium (99.99%, Sigma-Aldrich) was evaporated from a standard Knudsen cell onto the Ag(111) substrate, while keeping the substrate at room temperature. After deposition, the sample was annealed at 500 K for 1 h. Then the sample was transferred to the STM stage operating at 4 K. Pentacene (Sigma-Aldrich, purity 99%) and 7,7,8,8-tetracyanoquinodimethane (Sigma-Aldrich, purity 98%) were thermally deposited by a Knudsen 4-fold cell evaporator at 140 and 70 °C onto the monolayer Ag_5Se_2/Ag(111) substrate held at room temperature, respectively. For the codeposition different molecules experiment, the pentacene was firstly deposited onto the monolayer Ag_5Se_2/Ag(111) substrate held at room temperature and then the TCNQ was deposited onto the pentacene covered monolayer Ag_5Se_2/Ag(111) substrate held at room temperature. After deposition, the sample was transferred to the STM stage held at 4 K. All STM images were acquired in the constant-current mode, by using an electrochemically etched tungsten tip and the bias voltage was defined as the sample bias with respect to the tip. The Nanotec Electronica WSxM software was used to process the STM images shown here [28]. We performed q-Plus AFM imaging in a Createc low-temperature STM/AFM system with base pressure of 2.0×10^{-10} mbar at 4.5 K. The AFM images were obtained at constant height in frequency modulation (FM) mode. The qPlus sensor oscillated at an amplitude of 100 pm with a Q factor of 50,000. The resonance frequency was about 27.9 kHz, and the stiffness was about 1,800 N/m. The dI/dV spectra were recorded by a lock-in technique with a modulation amplitude of 10 mV and a frequency of 599 Hz.

First-principles calculations. DFT calculations were performed using the projector augmented wave (PAW) method with the local density approximation (LDA) functional [29], as implemented in the Vienna *ab initio* simulation package (VASP) code [30, 31]. The calculation cell contained a Ag-Se film on a three-layer Ag(111) substrate. A vacuum region of ~ 15 Å was applied and a plane-wave basis set with energy cutoff of 300 eV was used. The Brillouin zone was sampled by the Γ point. The structures were fully relaxed until energy and force on each atom were converged to 10^{-4} eV and 0.01 eV·Å^{-1}, respectively, while the bottom two layers of silver atoms were fixed. The simulated STM images were obtained using the constant current mode based on calculated electron densities.

Acknowledgements

This work was supported by the financial support from the National Key R&D Program of China (Nos. 2018YFA0305800 and 2019YFA0308500), National Natural Science Foundation of China (Nos. 61901200, 61925111, 61888102, and 21661132006), the Strategic Priority Research Program of Chinese Academy of Sciences (Nos. XDB30000000 and XDB28000000), the International Partnership Program of Chinese Academy of Sciences (No. 112111KYSB20160061), the KC Wong Education Foundation, the Yunnan Fundamental Research Projects (Nos. 2019FD041, 202201AT070078, and 202101AW070010), and the China Postdoctoral Science Foundation. Part of the research was performed in the Key Laboratory of Vacuum Physics, Chinese Academy of Sciences. Computational resources were provided by the National Supercomputing Center in Tianjin Municipality, China. Work at Vanderbilt University was supported by the U. S. Department of Energy, Office of Science, Basic Energy Sciences, Materials Science and Engineering Division grant No. DE-FG-02-09ER46554 and by the McMinn endowment.

Electronic Supplementary Material: Supplementary material (LEED analysis of the monolayer Ag_5Se_2 on Ag(111), other models of Se atoms adsorbed on Ag(111), detailed structure and stoichiometric ratio of monolayer Ag_5Se_2 on Ag(111), and qPlus AFM measurements of monolayer Ag_5Se_2 on Ag(111)) is available in the online version of this article at https://doi.org/10.1007/s12274-022-4314-6.

References

[1] Novoselov, K. S.; Geim, A. K.; Morozov, S. V.; Jiang, D.; Zhang, Y.; Dubonos, S. V.; Grigorieva, I. V.; Firsov, A. A. Electric field effect in atomically thin carbon films. *Science* **2004**, *306*, 666–669.

[2] Novoselov, K. S.; Geim, A. K.; Morozov, S. V.; Jiang, D.; Katsnelson, M. I.; Grigorieva, I. V.; Dubonos, S. V.; Firsov, A. A. Two-dimensional gas of massless Dirac fermions in graphene. *Nature* **2005**, *438*, 197–200.

[3] Geim, A. K.; Novoselov, K. S. The rise of graphene. *Nat. Mater.* **2007**, *6*, 183–191.

[4] Wang, Q. H.; Kalantar-Zadeh, K.; Kis, A.; Coleman, J. N.; Strano, M. S. Electronics and optoelectronics of two-dimensional transition metal dichalcogenides. *Nat. Nanotechnol.* **2012**, *7*, 699–712.

[5] Gao, L.; Sun, J. T.; Lu, J. C.; Li, H.; Qian, K.; Zhang, S.; Zhang, Y. Y.; Qian, T.; Ding, H.; Lin, X. et al. Epitaxial growth of honeycomb monolayer CuSe with Dirac nodal line fermions. *Adv. Mater.* **2018**, *30*, 1707055.

[6] Fiori, G.; Bonaccorso, F.; Iannaccone, G.; Palacios, T.; Neumaier, D.; Seabaugh, A.; Banerjee, S. K.; Colombo, L. Electronics based on two-dimensional materials. *Nat. Nanotechnol.* **2014**, *9*, 768–779.

[7] Chhowalla, M.; Shin, H. S.; Eda, G.; Li, L. J.; Loh, K. P.; Zhang, H. The chemistry of two-dimensional layered transition metal dichalcogenide nanosheets. *Nat. Chem.* **2013**, *5*, 263–275.

[8] Mak, K. F.; Shan, J. Photonics and optoelectronics of 2D semiconductor transition metal dichalcogenides. *Nat. Photon.* **2016**, *10*, 216–226.

[9] Wang, X. Y.; Zhang, H.; Ruan, Z. L.; Hao, Z. L.; Yang, X. T.; Cai, J. M.; Lu, J. C. Research progress of monolayer two-dimensional atomic crystal materials grown by molecular beam epitaxy in ultra-high vacuum conditions. *Acta Phys. Sin.* **2020**, *69*, 118101.

[10] Wang, X. Y.; Ruan, Z. L.; Du, R. J.; Zhang, H.; Yang, X. T.; Niu, G. F.; Cai, J. M.; Lu, J. C. Structural characterizations and electronic properties of CuSe monolayer endowed with triangular nanopores. *J. Mater. Sci.* **2021**, *56*, 10406–10413.

[11] Zhang, Y.; Chang, T. R.; Zhou, B.; Cui, Y. T.; Yan, H.; Liu, Z. K.; Schmitt, F.; Lee, J.; Moore, R.; Chen, Y. L. et al. Direct observation of the transition from indirect to direct bandgap in atomically thin epitaxial $MoSe_2$. *Nat. Nanotechnol.* **2014**, *9*, 111–115.

[12] Lu, J. C.; Bao, D. L.; Qian, K.; Zhang, S.; Chen, H.; Lin, X.; Du, S. X.; Gao, H. J. Identifying and visualizing the edge terminations of single-layer $MoSe_2$ island epitaxially grown on Au(111). *ACS Nano* **2017**, *11*, 1689–1695.

[13] Lu, Q. P.; Yu, Y. F.; Ma, Q. L.; Chen, B.; Zhang, H. 2D transition-metal-dichalcogenide-nanosheet-based composites for photocatalytic and electrocatalytic hydrogen evolution reactions. *Adv. Mater.* **2016**, *28*, 1917–1933.

[14] Wang, H. T.; Lu, Z. Y.; Xu, S. C.; Kong, D. S.; Cha, J. J.; Zheng, G. Y.; Hsu, P. C.; Yan, K.; Bradshaw, D.; Prinz, F. B. et al. Electrochemical tuning of vertically aligned MoS_2 nanofilms and its application in improving hydrogen evolution reaction. *Proc. Natl. Acad. Sci. USA* **2013**, *110*, 19701–19706.

[15] Panchakarla, L. S.; Subrahmanyam, K. S.; Saha, S. K.; Govindaraj, A.; Krishnamurthy, H. R.; Waghmare, U. V.; Rao, C. N. R. Synthesis, structure, and properties of boron- and nitrogen-doped graphene. *Adv. Mater.* **2009**, *21*, 4726–4730.

[16] Garnica, M.; Stradi, D.; Barja, S.; Calleja, F.; Díaz, C.; Alcamí, M.; Martín, N.; De Parga, A. L. V.; Martín, F.; Miranda, R. Long-range magnetic order in a purely organic 2D layer adsorbed on epitaxial graphene. *Nat. Phys.* **2013**, *9*, 368–374.

[17] Voiry, D.; Goswami, A.; Kappera, R.; E Silva, C. D. C. C.; Kaplan, D.; Fujita, T.; Chen, M. W.; Asefa, T.; Chhowalla, M. Covalent functionalization of monolayered transition metal dichalcogenides by phase engineering. *Nat. Chem.* **2015**, *7*, 45–49.

[18] Kumar, A.; Banerjee, K.; Liljeroth, P. Molecular assembly on two-dimensional materials. *Nanotechnology* **2017**, *28*, 082001.

[19] Zhou, H. T.; Zhang, L. Z.; Mao, J. H.; Li, G.; Zhang, Y.; Wang, Y. L.; Du, S. X.; Hofer, W. A.; Gao, H. J. Template-directed assembly of pentacene molecules on epitaxial graphene on Ru(0001). *Nano Res.* **2013**, *6*, 131–137.

[20] Dil, H.; Lobo-Checa, J.; Laskowski, R.; Blaha, P.; Berner, S.; Osterwalder, J.; Greber, T. Surface trapping of atoms and molecules with dipole rings. *Science* **2008**, *319*, 1824–1826.

[21] Lin, X.; Lu, J. C.; Shao, Y.; Zhang, Y. Y.; Wu, X.; Pan, J. B.; Gao, L.; Zhu, S. Y.; Qian, K.; Zhang, Y. F. et al. Intrinsically patterned two-dimensional materials for selective adsorption of molecules and nanoclusters. *Nat. Mater.* **2017**, *16*, 717–721.

[22] Liu, Z. L.; Lei, B.; Zhu, Z. L.; Tao, L.; Qi, J.; Bao, D. L.; Wu, X.; Huang, L.; Zhang, Y. Y.; Lin, X. et al. Spontaneous formation of 1D pattern in monolayer VSe_2 with dispersive adsorption of Pt atoms for HER catalysis. *Nano Lett.* **2019**, *19*, 4897–4903.

[23] Arnold, F.; Stan, R. M.; Mahatha, S. K.; Lund, H. E.; Curcio, D.; Dendzik, M.; Bana, H.; Travaglia, E.; Bignardi, L.; Lacovig, P. et al. Novel single-layer vanadium sulphide phases. *2D Mater.* **2018**, *5*, 045009.

[24] Du, S. X.; Gao, H. J.; Seidel, C.; Tsetseris, L.; Ji, W.; Kopf, H.; Chi, L. F.; Fuchs, H.; Pennycook, S. J.; Pantelides, S. T. Selective nontemplated adsorption of organic molecules on nanofacets and the role of bonding patterns. *Phys. Rev. Lett.* **2006**, *97*, 156105.

[25] Wang, Y. L.; Li, L. F.; Yao, W.; Song, S. R.; Sun, J. T.; Pan, J. B.; Ren, X.; Li, C.; Okunishi, E.; Wang, Y. Q. et al. Monolayer $PtSe_2$, a new semiconducting transition-metal-dichalcogenide, epitaxially grown by direct selenization of Pt. *Nano Lett.* **2015**, *15*, 4013–4018.

[26] Lu, J. C.; Gao, L.; Song, S. R.; Li, H.; Niu, G. F.; Chen, H.; Qian, T.; Ding, H.; Lin, X.; Du, S. X. et al. Honeycomb AgSe monolayer nanosheets for studying two-dimensional dirac nodal line fermions. *ACS Appl. Nano Mater.* **2021**, *4*, 8845–8850.

[27] Patrick, D. L.; Cee, V. J.; Beebe, T. P. Jr. "Molecule corrals" for studies of monolayer organic films. *Science* **1994**, *265*, 231–234.

[28] Horcas, I.; Fernández, R.; Gómez-Rodríguez, J. M.; Colchero, J.; Gómez-Herrero, J.; Baro, A. M. WSXM: A software for scanning probe microscopy and a tool for nanotechnology. *Rev. Sci. Instrum.* **2007**, *78*, 013705.

[29] Kohn, W.; Sham, L. J. Self-consistent equations including exchange and correlation effects. *Phys. Rev.* **1965**, *140*, A1133–A1138.

[30] Kresse, G.; Furthmüller, J. Efficiency of *ab-initio* total energy calculations for metals and semiconductors using a plane-wave basis set. *Comput. Mater. Sci.* **1996**, *6*, 15–50.

[31] Kresse, G.; Furthmüller, J. Efficient iterative schemes for *ab initio* total-energy calculations using a plane-wave basis set. *Phys. Rev. B* **1996**, *54*, 11169–11186.